Received: 12 October 2021 | Revised: 8 November 2021 | Accepted: 8 November 2021

DOI: 10.1002/pol.20210763

RESEARCH ARTICLE

JOURNAL OF POLYMER SCIENCE WILEY

Physically intuitive continuum mechanics model for quartz crystal microbalance: Viscoelasticity of rubbery polymers at MHz frequencies

Yannic J. Gagnon | **Justin C. Burton** | **Connie B. Roth**

Department of Physics, Emory University, Atlanta, Georgia, USA

Correspondence
Justin C. Burton and Connie B. Roth, Department of Physics, Emory University, Atlanta, GA 30322 USA.
Email: justin.c.burton@emory.edu; cbroth@emory.edu

Funding information
Division of Materials Research, Grant/Award Number: DMR-1905782

Abstract

Employing a quartz crystal microbalance (QCM) as a MHz-viscoelastic sensor requires extracting information from higher harmonics beyond the Sauerbrey limit, which can be problematic for rubbery polymer films that are highly dissipative because of the onset of anharmonic side bands and film resonance. Data analysis for QCM can frequently obscure the underlying physics or involve approximations that tend to break down at higher harmonics. In this study, modern computational tools are leveraged to solve a continuum physics model for the QCM's acoustic shear wave propagation through a polymer film with zero approximations, retaining the physical intuition of how the experimental signal connects to the shear modulus of the material. The resulting set of three coupled equations are solved numerically to fit experimental data for the resonance frequency Δf_n and dissipation $\Delta\Gamma_n$ shifts as a function of harmonic number n, over an extended harmonic range approaching film resonance. This allows the frequency-dependent modulus of polymer films at MHz frequencies, modeled as linear on a log–log scale, to be determined for rubbery polybutadiene (PB) and polydimethylsiloxane (PDMS) films, showing excellent agreement with time–temperature shifted rheometry data from the literature.

KEYWORDS

polymer thin films, quartz crystal microbalance, rheology, viscoelasticity

1 | INTRODUCTION

Quartz crystal microbalances (QCMs), though originally employed primarily as mass sensors, are increasingly being used to measure the MHz-frequency viscoelastic properties of a wide range of polymer film and brush systems in the nm–μm thickness range.[1–22] The viscoelastic properties of these systems at such high frequencies are important for sound damping and acoustic impedance matching applications at ultrasonic frequencies where rubbery polymer films near their glass transition regime exhibit high loss.[23–25] To access such viscoelastic properties of materials via QCM, one needs to go beyond the well-known Sauerbrey region at low harmonic numbers that is primarily sensitive to only the mass added to the QCM sensor.

At low harmonic numbers n, the frequency shift Δf_n of the QCM resonance is given by the Sauerbrey equation[2,26]:

$$\frac{\Delta f_n^{\text{Sauerbrey}}}{f_0} = -\frac{2f_0}{Z_q}(\rho h)\, n, \tag{1}$$

where for a film of thickness h and density ρ, (ρh) is the mass per unit area of the film placed on the sensor. The

fundamental frequency f_0 at $n = 1$ and the acoustic impedance Z_q are both properties of the quartz sensor being used. To access the film's viscoelastic properties, QCM measurements must be conducted at higher harmonics beyond the linear n-dependence of the Sauerbrey regime, as well as incorporating dissipation data, related to the bandwidth of the resonance. Going to higher harmonic numbers n, however, can be problematic, especially for more dissipative systems like rubbery polymers where the emergence of anharmonic side bands and the onset of film resonance occur at lower harmonics, imposing limits on the maximum frequency accessible. Film resonance occurs when the formation of standing acoustic waves in the film result in large amplitude oscillations.[2,12] Standard QCM analysis methods typically simplify equations to facilitate analytical solutions,[27] but this can further limit the maximum harmonic number accessible. As such, more recent methods favor numerical solutions to equations with fewer approximations.[1,2] As discussed by the Shull group,[9] the relevant quantity for evaluating deviations from the Sauerbrey regime and determining the viability of viscoelastic measurements via QCM is the ratio of the film thickness h to the wavelength of the shear wave λ_n:

$$\frac{h}{\lambda_n} = \frac{hf_n}{\Re(\tilde{c})} = h(nf_0)\sqrt{\frac{\rho}{|\tilde{G}|}}\cos(\phi/2) \tag{2}$$

where the complex speed of sound in the material $\tilde{c} = \sqrt{\tilde{G}/\rho}$ depends on the film's complex modulus $\tilde{G} = G' + iG'' = |\tilde{G}|\, e^{i\phi}$ and density ρ. Values of $\frac{h}{\lambda_n}$ from 0.05 to 0.20 are found to provide the optimal range for viscoelastic measurements.[9,12] Thus, depending on the modulus of the material, the film thickness should ideally be chosen to maximize the small window of accessible harmonics spanning from the end of the Sauerbrey regime to the beginning of film resonance where QCM will be sensitive to the film's viscoelasticity.

To obtain the viscoelastic properties of a film, one of two approaches to QCM modeling is typically used. The first approach, which dates back to the late 1990s and is the basis for the viscoelastic model in QCM-D systems, uses a continuum mechanics analysis while treating the film layers as a Kelvin-Voigt material.[3,28] The Kelvin-Voigt spring-dashpot model for a viscoelastic solid combines a spring element $\hat{G}$ in parallel with a dashpot element $\hat{\eta}$ resulting in a frequency-independent storage modulus $G'(f) = \hat{G}$ and a loss modulus with a linear dependence on frequency $G''(f) = 2\pi f\hat{\eta}$.[3,27] Depending on the material in question, this generic frequency dependence for a viscoelastic material can be inappropriate at the frequency range of the QCM,[1,27] as such recent methods typically incorporate a more general frequency dependence in an extended Voigt model.[1,3,29] The second approach treats the load on the QCM using an acoustic multilayer formalism developed and refined from the 1950s–1990s, where an equivalent circuit model is used to solve for the acoustic impedance of the QCM-film system from which the viscoelastic properties of the film can be extracted.[30,31] Although powerful, this method can obscure the connection between the underlying physics and the properties of the material being studied. The book by Johannsmann,[27] as well as several excellent reviews,[1–3,31,32] provide a useful summary of the history and range of systems studied with QCM operating as a MHz-frequency rheometer. In addition to these more conventional methods of QCM analysis, recent work by the Shull group has used an acoustic impedance-based model to numerically fit the ratio of frequency and dissipation shifts measured at two different harmonics to determine the viscoelastic modulus for a range of glassy and rubbery polymers.[1,7–10,12,13,33] This method is based on the Lu-Lewis[34] equation that matches the load impedance $\tilde{Z}_L$ at the resonator's surface with that caused by the film at the quartz/film interface.[1,2]

With these modeling efforts in mind, two main challenges confront the QCM user interested in investigating the viscoelastic properties of rubbery polymer films: to maintain the underlying physics intuition of the QCM model, while not introducing approximations that limit the frequency range of the measurement. In the present work, we leverage modern computational tools to numerically solve a physically intuitive continuum physics model for the shear wave propagation of the QCM's acoustic wave through the sample. This allows us to fit resonance frequency Δf_n and dissipation $\Delta\Gamma_n$ shifts over a range of harmonics n without any approximations to determine the frequency dependent modulus $\tilde{G}(\omega) = G'(\omega) + iG''(\omega)$. We apply this method to rubbery films of polybutadiene (PB) and polydimethylsiloxane (PDMS), as well as glassy polystyrene (PS), comparing the QCM measured MHz-frequency viscoelasticity with time–temperature shifted rheometry data from the literature.

2 | EXPERIMENTAL METHODS

Polystyrene (PS) (M_w = 1920 kg/mol, M_w/M_n = 1.26) from Pressure Chemical and polybutadiene (PB) (M_w = 375 kg/mol, M_w/M_n = 2.4; 36% cis 1,4; 55% trans 1,4; 9% vinyl 1,2, as specified by the supplier) from Scientific Polymer Products were purchased and used as received. Both the PS and PB samples were spin-coated from toluene solutions directly onto the QCM sensor, as well as silicon pieces for film thickness determination by ellipsometry. Films were annealed under vacuum for a minimum of 14 h after

spin-coating at a temperature of 120 °C for PS ($T_g \approx 100$ °C) and 25 °C for PB ($T_g \approx -96$ °C) to remove residual solvent and release stresses developed during spin-coating. Polydimethylsiloxane (PDMS) films cross-linked at a base to cross-linker ratio of 9:1 by mass were prepared using the Sylgard 184 kit manufactured by Dow Corning. After mixing the base and cross-linking agent for ≈1 min, the PDMS mixture was diluted with heptane for spin-coating (at ≈30 wt% of the PDMS mixture in heptane).[35] PDMS films were then cured at 70 °C for 2 h to match the curing schedule of Refs. 35–37.

Film thicknesses were determined by spin-coating films sequentially onto a silicon wafer, the QCM sensor, and then another silicon wafer. Ellipsometry was used to provide an independent measure of the film thickness on the QCM sensor by averaging the values obtained for the films on the silicon wafers. The thickness of the film on the QCM sensor was also determined by fitting the frequency Δf_n and dissipation $\Delta\Gamma_n$ shifts to the continuum physics model, where good agreement was found with the ellipsometry measurements.

Ellipsometry measurements were conducted using a J. A. Woollam M-2000 variable angle spectroscopic ellipsometer with rotating compensator. The film thickness h and index of refraction $n(\lambda)$ for the polymer layer were determined by fitting the amplitude $\Psi(\lambda)$ and phase shift $\Delta(\lambda)$ ellipsometry data, corresponding to the complex intensity ratio of p- to s-polarized light, collected at three angles of incidence (55°, 60°, and 65°) over the wavelength range λ spanning 400–1000 nm to an optical layer model using Woollam's CompleteEASE software. The optical layer model was comprised of a transparent Cauchy layer $n(\lambda) = A + \frac{B}{\lambda^2} + \frac{C}{\lambda^4}$ for the polymer film, atop a semi-infinite silicon substrate with a 1.25 nm native oxide layer.[38] For ellipsometric modeling of spin-coated PDMS films, an additional thickness non-uniformity parameter was included in the fit, with values typically between 3% and 7%.[35]

For the QCM measurements, AT-cut quartz sensors from Stanford Research Systems with a fundamental frequency f_0 of 5 MHz were used. Individual resonance peaks were collected with a vector network analyzer (Agilent 4395a) driving the system at 0 dBm, corresponding to a power of 1 mW. The circuit diagram of how the QCM sensor was connected to the network analyzer is given in Figure 1. All QCM measurements were done at room temperature (25 °C). For rubbery PB and PDMS films, full resonance traces were collected for a range of harmonics from $n = 1$ up to $n = 13$. The maximum harmonic number n for each film was limited by the emergence of anharmonic side peaks,[27] as described in section 3.3.3. Additional control measurements on glassy PS films were done where only the resonance frequencies f_n were measured for harmonics $n = 1$–19.

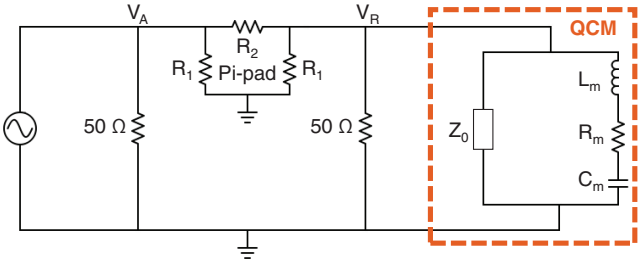

FIGURE 1 Circuit model for the QCM setup connected to the network analyzer. The QCM sensor, holder, and associated cables are highlighted by the orange dashed box. Their components consist of the motional branch elements L_m, R_m, and C_m in parallel with the electrical parasitic impedance Z_0. The network analyzer provides an oscillating voltage and measures V_A and V_R at its ports, each of which passes through a 50 Ω internal resistor to ground. A Pi-pad attenuator that includes resistors R_1 and R_2 separate V_A and V_R

The measured resonance traces were fit to a nonlinear functional form determined from an analysis of the QCM circuit to find the resonance frequency f_n and dissipation Γ_n at each harmonic. Figure 1 shows the circuit diagram of the QCM equivalent circuit connected to the network analyzer with a Pi-pad attenuator consisting of resistors R_1 and R_2. The QCM equivalent circuit, identified by the dashed box in the figure, consists of a motional branch with values L_m, R_m, and C_m, describing the mechanical properties of the QCM sensor. An additional electrical branch, with a parasitic impedance Z_0 is included to account for the parasitic capacitances of the QCM's electrodes and holder, and the parasitic capacitances and inductances of the cables and connections used to connect the QCM to the network analyzer. The voltages identified as V_A and V_R are measured at the ports of the network analyzer, each of which passes through an internal resistance of 50 Ω to ground. The V_A and V_R voltages themselves are separated by a Pasternack 50 Ω, −3 dBm, Pi-pad attenuator, which was added to decrease the source power by half and to reduce electronic reflections.

The data collected from the analyzer is in the form $20\log_{10}|\frac{V_A}{V_R}|$. Solving for $\frac{V_A}{V_R}$ in the circuit diagram shown in Figure 1 by adding impedances in series and parallel gives the following functional form for the attenuator signal:

$$20\log_{10}\left|\frac{V_A}{V_R}\right| = V_{\text{off}} + 10\log_{10}\left[C^2 + B_n^2 f^2 + \frac{A_n^2 + 2CA_n - B_n A_n\left(f^2 - f_n^2\right)/\Gamma_n}{1 + \left(f^2 - f_n^2\right)^2/\left(4\Gamma_n^2 f^2\right)}\right] \quad (3)$$

The parameter $C = 1 + R_2\left(\frac{1}{R_1} + \frac{1}{50\,\Omega}\right) = 1.41$ since $R_1 = 292.4\ \Omega$ and $R_2 = 17.6\ \Omega$. The parameters $A_n = \frac{R_2}{R_m}$ and $B_n = 2\pi R_2 Z_0$ both change with harmonic number n as the motional resistance R_m of the QCM sensor and the parasitic

impedance of the circuit Z_0 vary with frequency. We additionally observed a non-zero background in the network analyzer data, which we determined to be due primarily to electromagnetic wave reflections in the cables and connections. This background is constant within the small frequency range of an individual harmonic. We therefore added a constant vertical offset term V_{off} to Equation (3) to account for vertical shifts in the background at each harmonic. This leaves us with five fitting parameters to fit the resonance peak, where f_n corresponds to the peak frequency and Γ_n the bandwidth, A_n corresponds to the amplitude of the peak while B_n accounts for its asymmetry, and V_{off} corrects for any baseline offsets.

Figure 2 shows resonance peaks for a 250 nm thick PB film atop the QCM sensor collected at harmonic numbers $n = 3$ ($f_3 = 3f_0 = 15$ MHz) and $n = 9$ ($f_9 = 9f_0 = 45$ MHz). Fits of Equation (3) to these resonance peaks give best fit parameter values of $f_3 = 15.0169$ MHz $\pm$ 0.06 Hz and $\Gamma_3 = (69.21 \pm 0.06)$ Hz, with $A_3 = 0.5162 \pm 0.0003$, $B_3 = (-3.62 \pm 0.06) \times 10^{-9}$ Ω^2, and $V_{off} = 0.0089 \pm 0.0004$ dBm for $n = 3$, and $f_9 = 45.0432$ MHz $\pm$ 0.3 Hz and $\Gamma_9 = (691.9 \pm 0.3)$ Hz, with $A_9 = 0.04979 \pm 0.00001$, $B_9 = (-3.44 \pm 0.01) \times 10^{-9}$ Ω^2, and $V_{off} = (-0.0322 \pm 0.0003)$ dBm for $n = 9$. Similar resonance traces were collected from other samples and fit with Equation (3), where the error associated with measuring any individual resonance peak was always smaller than the sample-to-sample variability. For a given polymer film, the resonance peaks collected at higher harmonics show a decreased peak amplitude A_n and increased peak width Γ_n caused by the increased viscous dissipation at higher frequencies.

When a polymer film is added to the QCM sensor, the motional branch elements of the QCM are altered causing a shift in the resonance frequency $f_n = \frac{1}{2\pi\sqrt{L_m C_m}}$ and dissipation $\Gamma_n = \frac{R_m}{4\pi L_m}$, relative to that of the bare quartz. To determine the shifts in frequency $\Delta f_n = f_n^{\text{film+QCM}} - f_n^{\text{bare QCM}}$ and dissipation $\Delta\Gamma_n = \Gamma_n^{\text{film+QCM}} - \Gamma_n^{\text{bare QCM}}$, measurements of the resonance peaks were collected for both the bare quartz initially giving $f_n^{\text{bare QCM}}$ and $\Gamma_n^{\text{bare QCM}}$, and then the same quartz sensor with the film added giving $f_n^{\text{film+QCM}}$ and $\Gamma_n^{\text{film+QCM}}$. These frequency and dissipation shifts, Δf_n and $\Delta\Gamma_n$, between the film-loaded and bare quartz QCM sensors are the main parameters we are interested in for the analysis with our continuum physics model.

3 | RESULTS AND DISCUSSION

3.1 | Continuum physics model and numerical fitting

We present a continuum physics QCM model for a linear viscoelastic polymer film with a complex, frequency

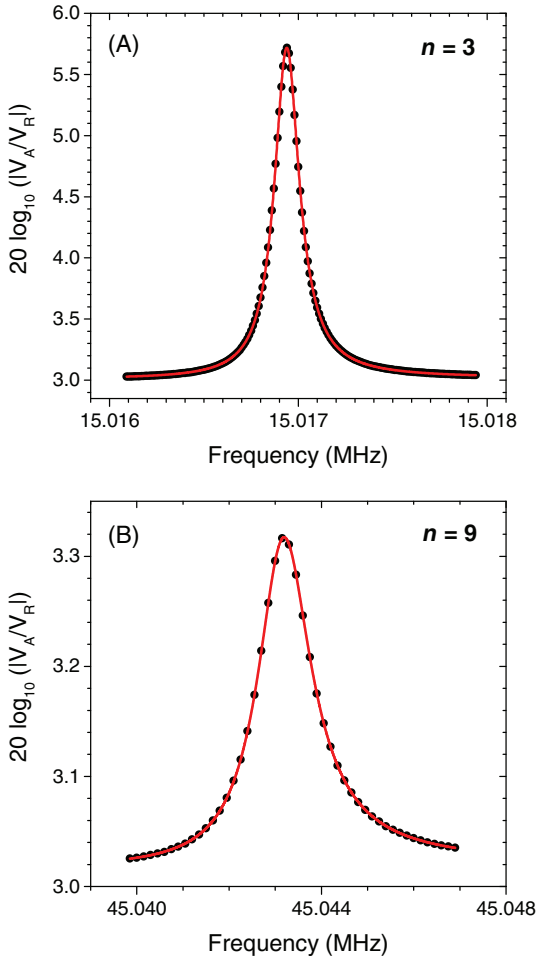

FIGURE 2 Resonance peaks for a 250 nm thick PB film on a QCM sensor at the $n = 3$ harmonic (A) and the $n = 9$ harmonic (B). The red curves represent fits of equation (3) to the data (black symbols), which are used to measure the frequency f_n and dissipation Γ_n for each resonance

dependent shear modulus $\tilde{G}(\omega) = G'(\omega) + iG''(\omega)$ that preserves the simple intuitive physics of the sample geometry and can be solved numerically without any approximations using current scientific computer programs such as Mathematica. This model is quantitatively equivalent to the more commonly used Lu-Lewis equation that is also solved numerically,[1,2] but physicists familiar with continuum mechanics may find this derivation more intuitive. For a viscoelastic film atop AT-cut quartz crystals, the QCM oscillation can be readily treated as a one-dimensional shear wave propagating away from the QCM surface, as the thickness shear mode in the plane of the film is dominant and compressional oscillations can be ignored. This is commonly referred to as the parallel plate model, where energy trapping considerations are ignored, see Ref. [2] for a more complete discussion.

Figure 3 illustrates our sample geometry with axes for the model, where we treat the shear wave as propagating in the z-direction and oscillating in the y-direction. The shear

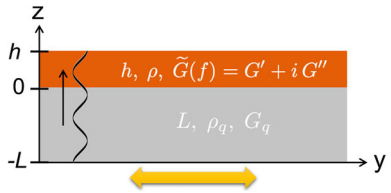

FIGURE 3 Layer geometry for the continuum physics model illustrating the one-dimensional shear wave propagating from the QCM quartz surface into the polymer film along the z-direction. A polymer film of thickness h, density ρ, and shear modulus $\widetilde{G}(f) = G'(f) + iG''(f)$ is placed atop the quartz resonator of thickness L, density ρ_q, and shear modulus G_q

wave displacement in the $\hat{y}$ - direction for the polymer film $\vec{u}_f$ and quartz crystal $\vec{u}_q$ can be written as

$$\vec{u}_f(z,t) = e^{-i\widetilde{\omega}t}\left(A_f\, e^{i\widetilde{k}_f z} + B_f\, e^{-i\widetilde{k}_f z}\right)\hat{y} \quad \text{(film layer)} \tag{4}$$

$$\vec{u}_q(z,t) = e^{-i\widetilde{\omega}t}\left(A_q\, e^{i\widetilde{k}_q z} + B_q\, e^{-i\widetilde{k}_q z}\right)\hat{y} \quad \text{(quartz layer)} \tag{5}$$

where $\widetilde{k}_i = 2\pi\widetilde{f}/\widetilde{c}_i$ is the complex wave vector, and A_i and B_i are the wave amplitudes of the forward propagating and reflected waves, respectively.

The complex angular frequency $\widetilde{\omega} = 2\pi\widetilde{f} = 2\pi(f_n + i\Gamma_n)$ contains the information about the resonance frequency f_n and dissipation Γ_n of the film+quartz system at each harmonic number n. These resonance frequencies and dissipations of the film+quartz system are defined in the model based on the bare quartz oscillation as $f_n = nf_0 + \Delta f_n$ and $\Gamma_n = n\Gamma_0 + \Delta\Gamma_n$, allowing us to directly extract the frequency and dissipation shifts Δf_n and $\Delta\Gamma_n$. These quantities will then be fit to the experimentally determined values from the resonance traces, where Δf_n corresponds to the shift in peak position and $\Delta\Gamma_n$ corresponds to the change in peak width relative to that measured for the bare quartz.

The displacement in the polymer film for the transverse shear wave emanating from the quartz surface will satisfy the wave equation for an incompressible material[39]

$$\rho\frac{\partial^2\vec{u}_f}{\partial t^2} = \widetilde{G}\nabla^2\vec{u}_f \tag{6}$$

and similarly for the quartz layer. The speed for this shear wave is the transverse speed of sound $\widetilde{c} = \sqrt{\frac{\widetilde{G}}{\rho}}$ that depends on the material's shear modulus and density. Assuming Hooke's law for the linear viscoelastic polymer film under small shear displacement, the shear stress tensor for the continuous material under shear deformation can be written as[39]

$$\sigma_{yz} = 2\,\widetilde{G}\,U_{yz}, \tag{7}$$

where U_{yz} is the yz component of the strain tensor

$$U_{yz} = \frac{1}{2}\left(\frac{\partial u_z}{\partial y} + \frac{\partial u_y}{\partial z}\right). \tag{8}$$

For the AT-cut quartz sensor, the predominant oscillation is the thickness shear mode that is traveling in the z-direction and polarized in the y-direction, allowing us to neglect any compressional oscillation in the z-direction so that $u_z = 0$. This simplifies the strain and stress tensors to

$$U_{yz} = \frac{1}{2}\frac{\partial u_y}{\partial z} \quad \text{and} \quad \sigma_{yz} = \widetilde{G}\frac{\partial u_y}{\partial z} \tag{9}$$

where $u_y = \vec{u}_f$ in the polymer film. Similar equations exist for the quartz layer where $u_y = \vec{u}_q$, and ρ_q and G_q are normally written in terms of the acoustic impedance $Z_q = \sqrt{\rho_q G_q} = 8.8\times10^9$ g m^{-2} Hz for AT-cut quartz.[27]

To solve the system, we apply standard boundary conditions at the interfaces between the layers. Continuity of displacement at the film/quartz interface (no-slip boundary condition) gives

$$\begin{aligned} &u_f(z,t)\big|_{z=0} = u_q(z,t)\big|_{z=0} \\ &A_f + B_f = A_q + B_q. \end{aligned} \tag{10}$$

Stress continuity (Newton's third law) at the film/quartz interface gives

$$\begin{aligned} &\sigma_f(z,t)\big|_{z=0} = \sigma_q(z,t)\big|_{z=0} \\ &\sqrt{\rho\,\widetilde{G}}(A_f - B_f) = Z_q\,(A_q - B_q), \end{aligned} \tag{11}$$

while the top film/air and bottom quartz/air interfaces will be stress free giving

$$\begin{aligned} &\sigma_f(z,t)\big|_{z=h} = 0 \\ &A_f - B_f \exp\left[-i4\pi h\sqrt{\frac{\rho}{\widetilde{G}}}\,(f_n + i\Gamma_n)\right] = 0 \end{aligned} \tag{12}$$

and

$$\sigma_q(z,t)\big|_{z=-L} = 0$$
$$A_q - B_q \exp\left[i\frac{2\pi}{f_0}(f_n + i\Gamma_n)\right] = 0. \quad (13)$$

For computational simplicity, we are ignoring the tiny stress contribution due to air at these interfaces, which we estimate using Navier–Stokes to be less than a 0.03% correction on the frequency shift. Note, Equation (13) was simplified by recognizing that the thickness of the quartz crystal $L = \frac{\lambda_0}{2}$ is related to the fundamental frequency $f_0 = \frac{c_q}{\lambda_0}$ such that $\frac{L}{c_q} = \frac{1}{2f_0}$. This system of equations can then be further simplified by using Equation (10) to eliminate one of the displacement amplitudes, which we did to remove A_f. In addition, we also normalized the remaining amplitudes by setting $A_q = 1$ nm.

The continuum physics model can only account for the frequency Δf_n and dissipation $\Delta\Gamma_n$ shifts due to the presence of the polymer film relative to the idealized bare quartz resonance of $f_n = nf_0$ with $\Gamma_0 = 0$. As such Equations (12) and (13) need to be recast in terms of $\Delta f_n = f_n - nf_0$ and $\Delta\Gamma_n = \Gamma_n - \Gamma_0 \approx \Gamma_n$ by replacing $(f_n + i\Gamma_n) = (nf_0 + \Delta f_n + i\Delta\Gamma_n)$. Experimental factors associated with the circuit cables and QCM sensor mounting that might impact the frequency and dissipation measured in practice will be accounted for by determining the experimental frequency Δf_n and dissipation $\Delta\Gamma_n$ shifts relative to those measured directly for the bare quartz at each resonance:

$$\Delta f_n = f_n^{\text{film+QCM}} - f_n^{\text{bare QCM}} \quad (14)$$

$$\Delta\Gamma_n = \Gamma_n^{\text{film+QCM}} - \Gamma_n^{\text{bare QCM}} \quad (15)$$

Thus for the continuum physics model, this leaves us with a system of three complex equations that can be solved numerically using standard root finding methods to determine the complex frequency shift $\Delta\widetilde{f}_n = \Delta f_n + i\Delta\Gamma_n$ for a given polymer film of thickness h, density ρ, and a complex frequency-dependent shear modulus $\widetilde{G}(f_n)$:

$$\sqrt{\rho\,\widetilde{G}}\left(1 + B_q - 2B_f\right) - Z_q\left(1 - B_q\right) = 0 \quad (16)$$

$$1 + B_q - B_f\left(1 + \exp\left[-i4\pi h\sqrt{\frac{\rho}{\widetilde{G}}}(nf_0 + \Delta f_n + i\Delta\Gamma_n)\right]\right) = 0 \quad (17)$$

$$1 - B_q \exp\left[i\frac{2\pi}{f_0}(\Delta f_n + i\Delta\Gamma_n)\right] = 0 \quad (18)$$

To account for small variations in the fundamental frequency f_0 based on the particular cut of a given QCM sensor, the value of f_0 in the model is taken to be the experimentally measured value for the bare quartz crystal prior to adding the polymer film.

For the set of three Equations (16)–(18), the harmonic number n functions as the independent variable, while Δf_n and $\Delta\Gamma_n$ are the dependent variables. A chi-squared minimization fitting routine is used to minimize the deviation between the experimentally measured Δf_n and $\Delta\Gamma_n$ values with those calculated numerically solving Equations (16)–(18) in Mathematica at each harmonic number n. The density of the polymer film ρ is treated as a constant with values for each polymer determined from the literature, leaving the polymer film thickness h and shear modulus $\widetilde{G}(f_n) = G'(f_n) + iG''(f_n)$ as the fitting parameters to determine for each polymer film.

The chi-squared minimization was performed using the gradient-descent local minimization routine FindMinimum in Mathematica, which executed a Levenberg–Marquardt routine. As long as the initial guesses for the fit parameters were physically reasonable, the local minimum obtained matched a computationally longer global minimization algorithm (a). The fitting errors for the best fit parameter values obtained were determined by calculating the maximum range of each parameter along the χ^2 distribution corresponding to one standard deviation (a 68.3% confidence interval).

To account for the frequency-dependent viscoelastic nature of the polymer shear modulus $\widetilde{G}(f_n) = G'(f_n) + iG''(f_n)$, while limiting the number of fitting parameters needed, we take advantage of the narrow frequency range of the QCM (5 MHz to 65 MHz) and treat the frequency dependence as linear on a log modulus versus log frequency scale. This type of simplification has been done by others previously.[9,27] Given that $f_n = nf_0 + \Delta f_n \approx nf_0$, we can write

$$G'(f_n) \approx G'(n) = G_{0'}\, n^{\beta'} \quad (19)$$

$$G''(f_n) \approx G''(n) = G_0''\, n^{\beta''} \quad (20)$$

which for log–log axes gives

$$\log_{10}G'(n) = \beta'\log_{10}n + \log_{10}G_0' \quad (21)$$

$$\log_{10}G''(n) = \beta''\log_{10}n + \log_{10}G_0'' \quad (22)$$

G_0' and G_0'' correspond to the values of the storage and loss modulus at the first harmonic $n = 1$ (5 MHz). β'

and β'' represent the slope of the storage and loss modulus frequency dependence on a log–log scale within the QCM frequency range. To minimize the number of fit parameters, we used time–temperature shifted rheological data from the literature to determine β' and β'' for each rubbery polymer based on the local slope of $\log_{10}G'$ and $\log_{10}G''$ versus $\log_{10}f$ data in the QCM frequency range, as described in sections 3.3 and 3.4. Thus, this leaves three fitting parameters, G_0', G_0'', and h, for the continuum physics model to define the frequency and dissipation shifts Δf_n and $\Delta\Gamma_n$.

3.2 | Continuum physics model applied to glassy polystyrene films

As a simple test case, we begin by applying our continuum physics model to glassy polystyrene (PS) films. At room temperature (25 °C), PS is well within its glassy plateau region at MHz frequencies with negligible dissipation such that the shear modulus of PS can be treated as simply a constant storage shear modulus $\widetilde{G}(f) = G'$, independent of frequency. Justification for this choice of analysis is included in Supporting Information, along with representative resonance traces for PS. Focusing on only the frequency shifts Δf_n, resonance peaks were collected for a 1.37 μm thick PS film at harmonic numbers $n = 1$ to 19. The resonance frequencies of the bare QCM resonator were also measured at the same harmonic numbers $n = 1$ to 19 prior to the polymer film being added to the QCM sensor. The resonance frequency shifts were then defined as $\Delta f_n = f_n^{\text{film+QCM}} - f_n^{\text{bare QCM}}$. Figure 4A plots these Δf_n values, normalized by the fundamental frequency $f_0 = 5$ MHz of the bare quartz, as a function of harmonic number n. To focus on the viscoelastic response of the film, we subtract off the frequency shift expected for the Sauerbrey regime $\Delta f_n^{\text{Sauerbrey}}$ from purely mass loading, plotting $\Delta f_n - \Delta f_n^{\text{Sauerbrey}}$ in Figure 4B. A second 1.26 μm thick PS sample is also included.

Our continuum physics model presented in section 3.1 was used to fit these experimental values of Δf_n as a function of harmonic number n to obtain the glassy shear modulus for PS giving $G' = 1.53 \pm 0.10$ GPa and a film thickness of $h = 1.37 \pm 0.01$ μm, assuming a constant density for PS of $\rho = 1.04$ g/cm^3 obtained from the literature.[40] This film thickness value determined from fitting the QCM data to the continuum physics model agrees well with the value of 1.33 ± 0.10 μm independently determined by ellipsometry. Measurements were repeated for a 1.26 μm thick PS film, where fits of the frequency shift Δf_n data gave best fit values of $G' = 1.83 \pm 0.07$ GPa and $h = 1.265 \pm 0.004$ μm. Both these QCM measurements on two separate PS films show good reproducibility. The glassy shear modulus values measured for PS with QCM over the frequency range of 5 MHz to 95 MHz agree well with literature values

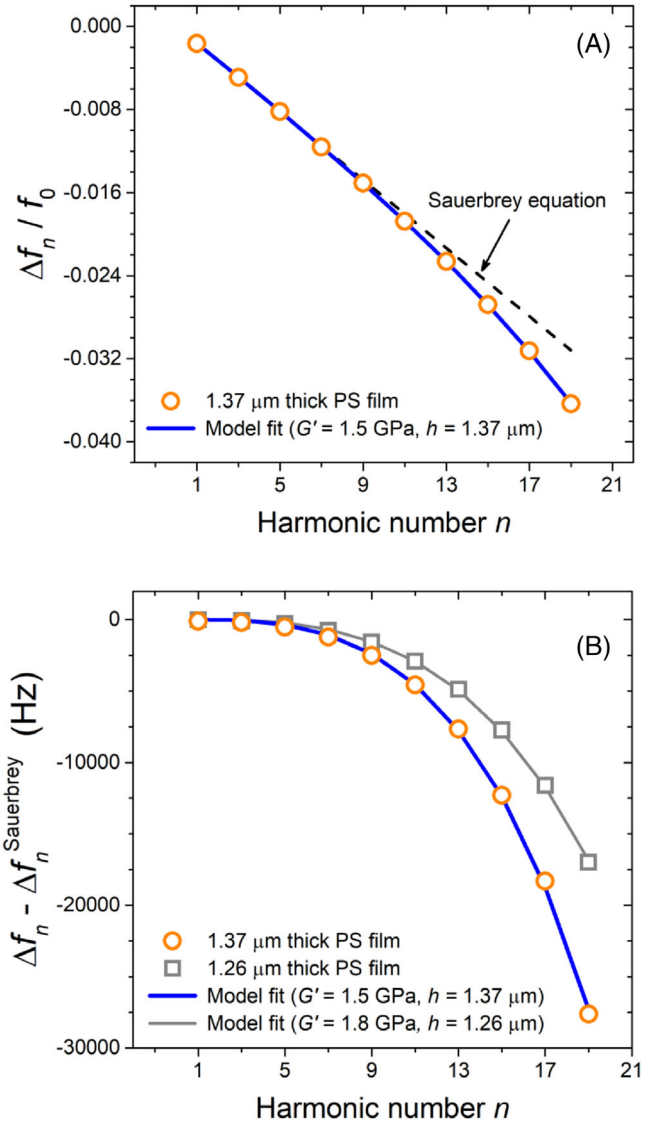

FIGURE 4 (A) Resonance frequency shifts Δf_n, normalized by the fundamental frequency f_0, measured by QCM at 25 °C over the harmonic range $n = 1$ to 19 (5 MHz to 95 MHz) for a PS film with a thickness of 1.37 μm (orange circles). These data were fit with our continuum physics model (blue curve) to determine the glassy shear modulus G' and film thickness h, giving $G' = 1.53 \pm 0.10$ GPa and $h = 1.37 \pm 0.01$ μm. The linear Sauerbrey region at low harmonics is indicated by the black dashed line, which is a linear fit to the data for the first three harmonics $n = 1, 3, 5$. (B) Frequency shifts Δf_n relative to the expected frequency shift from purely mass loading given by the Sauerbrey equation $\Delta f_n^{\text{Sauerbrey}}$, plotted as a function of harmonic number n for the 1.37 μm thick PS film and a second 1.26 μm thick PS film (gray squares). The continuum physics model fit (gray curve) to the data from this second sample give best fit values of $G' = 1.83 \pm 0.07$ GPa and $h = 1.265 \pm 0.004$ μm

for glassy PS storage modulus determined by QCM ($G' \approx 1/J' = 1.7$ GPa)[6] and measurements of the shear wave speed at 1 MHz ($G' = \rho c_s^2 = 1.3$ GPa and 1.4 GPa).[41–43] The agreement between our data and the model's fit, as well as the agreement between our G' values and those from the literature for glassy PS, verifies that our QCM experimental setup and modeling accurately describe the frequency response of a film with a glassy shear modulus on top of the QCM crystal.

3.3 | Continuum physics model applied to rubbery polybutadiene films

We now apply our continuum physics model to a fully viscoelastic rubbery polymer film, polybutadiene (PB), which is in its glass transition regime at 25 °C in the QCM MHz frequency range.[44–48] We therefore model the storage and loss moduli using Equations (21)–(22), which treat the frequency dependence of the shear modulus as linear on a log–log scale.

To minimize the number of fit parameters, we determined the local slope of $\log(G')$ and $\log(G'')$ versus $\log(f)$ within the QCM frequency range, corresponding to the exponents β' and β'' in Equations (21)–(22), by fitting rheological data from the literature.[44,45,47,48] These literature studies measured $G'(\omega)$ and $G''(\omega)$ (where $\omega = 2\pi f$) for PB samples at frequencies up to 100 rad/s (≈16 Hz) at different temperatures, then used time–temperature superposition to shift the moduli to a single reference temperature resulting in a collective frequency range spanning 10^{-3}–10^{+11} Hz. We digitized the data in the QCM frequency range from these studies corresponding to PB samples with molecular weights ranging from $M_w = 130$ kg/mol (Colby et al.[44]) to $M_w = 1200$ kg/mol (Liu et al.[48]). The data from Colby et al.[44] and Liu et al.[48] both used a reference temperature of 25 °C for their time–temperature superposition, while Palade et al.[45] and Wang et al.[47] used −85 °C and 40 °C reference temperatures, respectively. To superimpose the data from these literature studies on a single plot and compare them with our QCM results collected at room temperature (≈25 °C), we shifted the data from Palade et al.[45] and Wang et al.[47] to a reference temperature of 25 °C using the shift factors from their papers. We then performed linear fits to the $\log(G')$ and $\log(G'')$ versus $\log(f)$ data from each study for the frequency range from 5 MHz to 45 MHz (corresponding to QCM harmonic range of $n = 1$ to 9) resulting in best fit average and standard deviation values of $\beta' = 0.50 \pm 0.03$ for the storage and $\beta'' = 0.74 \pm 0.01$ for the loss moduli exponents. The small errors in β' and β'' illustrate the excellent agreement in the frequency dependence of the storage and loss moduli of PB over a wide range of molecular weights in the 5–45 MHz frequency range at the 25 °C reference temperature, within the glass transition regime. Given this consistency in β' and β'' values, it is reasonable to assume that these exponent values for the storage and loss moduli should apply well to our study's PB with a molecular weight of $M_w = 375$ kg/mol measured at room temperature by QCM within the glass transition regime. We therefore fix these exponent values of β' and β'' in our continuum model and fit our QCM data for the storage G_0' and loss G_0'' moduli offsets corresponding to $G'(n)$ and $G''(n)$ at $n = 1$ (5 MHz) in Equations (21)–(22), along with the film thickness h.

QCM measurements were conducted on PB films for a variety of film thicknesses ranging from 250 nm to 730 nm. Thicker films up to 2 μm were also investigated, but clear reliable resonance peaks could not be obtained. For each film measured, resonance traces were collected for a range of harmonics spanning from $n = 1$ up to $n = 13$. These resonance peaks were then fit with Equation (3), as described in the experimental methods section, to obtain the resonance frequency f_n and dissipation Γ_n at each harmonic n. Representative resonance traces for the harmonics at $n = 3$, 9, and 11 are shown in Figure 5A for a 250 nm thick PB film. Corresponding reference traces of the bare quartz crystal were also collected at each harmonic to determine the frequency shift $\Delta f_n = f_n^{\text{film+QCM}} - f_n^{\text{bare QCM}}$ and dissipation shift $\Delta\Gamma_n = \Gamma_n^{\text{film+QCM}} - \Gamma_n^{\text{bare QCM}}$. These values of Δf_n and $\Delta\Gamma_n$ are then plotted as a function of harmonic number n in Figure 5B, with similar results for a 510 nm thick PB film shown in Figure 5C. To focus on the viscoelastic response of these rubbery films, the frequency shift Δf_n is referenced to the frequency shift expected from the Sauerbrey equation resulting solely from the mass contribution $\Delta f_n^{\text{Sauerbrey}}$, as given by Equation (1).

As the harmonic number increases, especially for thicker films, anharmonic side peaks become present near the main resonance peak of interest. These side peaks are initially visible as side features far from the main resonance peak, but at sufficiently high harmonics, they eventually merge with the main resonance peak, rendering the fitting for f_n and Γ_n unreliable. Because of the caution often expressed about the presence of anharmonic side peaks,[27] it is common in the QCM literature to simply discard any resonance curves with side peaks in the vicinity of the main resonance peak or limit data to below some maximum harmonic number. In our measurements, we have identified resonance traces at higher n for which anharmonic side peaks appear to be present, but where we believe the main resonance peak can still be reliably fit to obtain f_n and Γ_n. An example of such a resonance trace is shown in Figure 5A for the $n = 11$

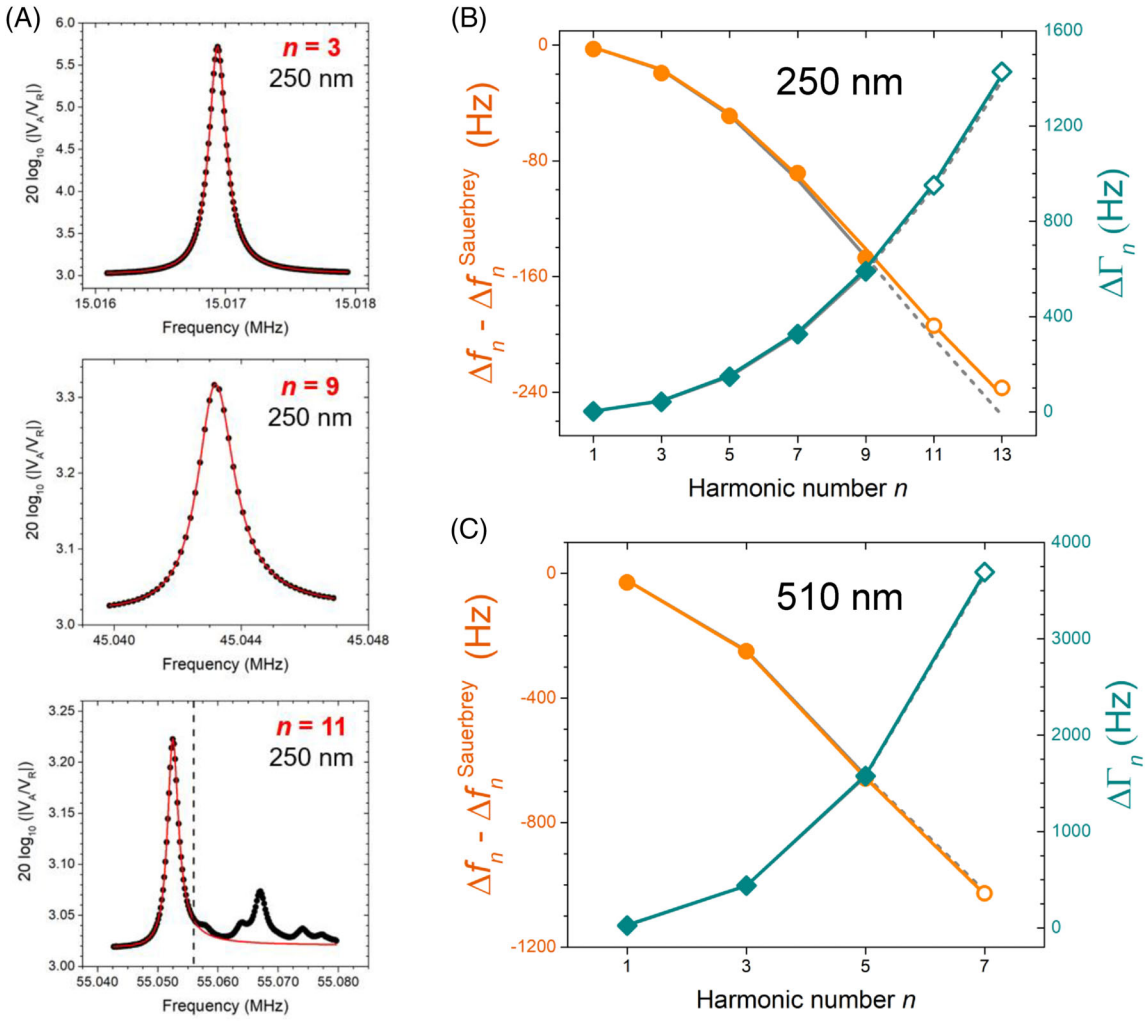

FIGURE 5 (A) Resonance traces of the $n = 3$, 9, and 11 harmonics for a 250 nm PB film on a QCM. The symbols are the data collected with the network analyzer and the red curves are fits using equation (3). The dashed vertical line in the $n = 11$ resonance plot corresponds to the maximum frequency used in fitting the resonance. Resonance frequency shifts Δf_n (orange circles, left axis) and dissipation shifts $\Delta\Gamma_n$ (teal diamonds, right axis) for a 250 nm (B) and 510 nm (C) PB film. The symbols are the experimental data and the curves the continuum physics model fits to these data, where the frequency shifts Δf_n have been referenced to that expected from the Sauerbrey equation $\Delta f_n^{\text{Sauerbrey}}$, which accounts only for the mass contribution. The solid-colored curves are a fit to both the solid and open symbols, while the gray solid and dashed curves are a fit to the solid symbols that are then extrapolated to higher harmonics, see text for details

harmonic of the 250 nm PB film. By limiting the fitting range to the main resonance peak, to the left of the vertical dashed line in the figure, we were able to obtain good fits to the main resonance peak. However, given the caution expressed with such traces, we have denoted the shifts obtained from the f_n and Γ_n values determined in this manner by open symbols in Figure 5B and 5C. f_n and $\Delta\Gamma_n$ shifts obtained from traces where no side peaks are present near the main resonance peak, such as those shown in Figure 5A for $n = 3$ and 9. We also find the resonance shifts at the fundamental harmonic $n = 1$ to be extremely reproducible and as reliable as the resonance shifts measured at $n = 3$, as such we have included the $n = 1$ data in our analysis.

In order to access the modulus of the polymer film, there would be benefits to maximizing the number of harmonics measured because the QCM resonance becomes more sensitive to the sample's viscoelasticity at higher harmonics. As we are solving our continuum physics model for the QCM numerically, we are not restricted to only low harmonics far from the film resonance condition, as would be necessary when using several of the approximations commonly used in QCM analysis. Thus, we can use our continuum physics model as a way of verifying the consistency of the frequency and dissipation shifts obtained from the higher harmonics with some adjacent side peaks present to the main resonance. We can do this by first using the continuum

physics model to fit only the solid symbols in Figure 5B and 5C, where no side peaks are present, and then extrapolating the model with these best fit parameters to higher harmonics to see how they compare with the Δf_n and $\Delta\Gamma_n$ values obtained when some adjacent side peaks are present (open symbols). From such a comparison, we find that the measured Δf_n and $\Delta\Gamma_n$ values (open symbols) are within 0.8% of the predicted values based on an extrapolation of the model. This good agreement suggests a consistency that justifies the inclusion of the higher harmonics (open symbols) where adjacent side peaks are present, but for which we believe the resonance and dissipation values can be accurately determined from the resonance trace. As such, we have chosen to fit the entire harmonic range measured (both open and solid symbols) to determine our best fit values for the storage and loss modulus of the polymer films by QCM. By comparing the curvature of the $\Delta f_n - \Delta f_n^{\text{Sauerbrey}}$ data as a function of harmonic number n with model predictions, we can identify these open symbols as occurring just near the start of the film resonance condition.

As described in section 3.1, the continuum physics model calculates the frequency and dissipation shifts Δf_n and $\Delta\Gamma_n$ as a function of harmonic number n expected for a polymer film supported on the QCM crystal based on its film thickness h, and storage $G'(n) = G'_0 n^{\beta'}$ and loss $G''(n) = G''_0 n^{\beta''}$ modulus values. By using literature data to fix the frequency dependence, exponent values β' and β'', we are left with only three fit parameters h, G'_0 and G''_0 that can be determined from fits of Δf_n and $\Delta\Gamma_n$ as a function of harmonic number n. The density of high molecular weight PB is between 0.894 and 0.896 g/cm^3 at room temperature;[44] in this study, we use the value of $\rho = 0.895$ g/cm^3 for our continuum model. For the 250 nm PB film shown in Figure 5B, the best fit values determined from a fit of all the data to our continuum physics model gives $h = 246 \pm 1$ nm for the film thickness, and $G'_0 = 2.64 \pm 0.66$ MPa and $G''_0 = 5.08 \pm 0.27$ MPa for the storage and loss modulus. For the 510 nm thick PB film shown in Figure 5C, the best fit values are $h = 510 \pm 2$ nm, and $G'_0 = 3.54 \pm 0.07$ MPa and $G''_0 = 4.07 \pm 0.08$ MPa. These film thickness values determined by QCM are in good agreement with the independently measured values by ellipsometry of $h = 244 \pm 3$ nm and $h = 531 \pm 16$ nm. Data were also collected for a thicker PB film of 730 nm thickness where fits of the QCM data for harmonics $n = 1$, 3, and 5 to the continuum physics model gave best fit values of $h = 732 \pm 6$ nm, and $G'_0 = 3.75 \pm 0.12$ MPa and $G''_0 = 4.12 \pm 0.19$ MPa, where again the QCM determined film thickness agreed well with the value independently measured by ellipsometry of $h = 765 \pm 4$ nm. To within experimental error, we do not observe any meaningful thickness dependence to the moduli values measured by QCM within the measured range of 250–730 nm.

Figure 6 graphs these best fit values of $G'(n) = G'_0 n^{0.50}$ and $G''(n) = G''_0 n^{0.74}$ for the three PB film thicknesses measured: 250 nm, 510 nm, and 730 nm. The error bars plotted include the fitting error of G'_0 and G''_0 added in quadrature to the uncertainty in G'_0 and G''_0 due to the range in the exponent values $\beta' = 0.50 \pm 0.03$ and $\beta'' = 0.74 \pm 0.01$. To facilitate comparison with the literature rheometry data for PB, the values are graphed as $\log G'(f)$ and $\log G''(f)$ versus the logarithm of the frequency $f = nf_0$. The literature data described above and used to determine the exponents β' and β'' over the QCM

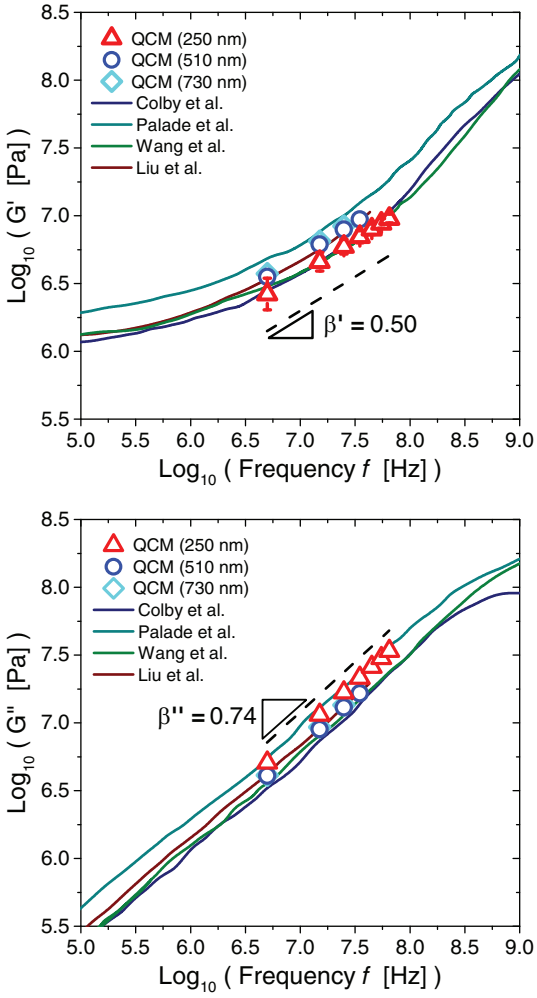

FIGURE 6 Log–log plot of storage $G'(f)$ and loss $G''(f)$ moduli for PB at 25 °C. Open symbols are the QCM data measured for PB ($M_w = 375$ kg/Mol) films with thicknesses of 250 nm (red triangles), 510 nm (blue circles), and 730 nm (cyan diamonds). Curves depict the literature rheometry data time–temperature shifted up to the MHz frequencies of the QCM.[44,45,47,48] The dashed lines show the local slope from 5–45 MHz averaged over all the literature studies giving the exponent values $\beta' = 0.50 \pm 0.03$ and $\beta'' = 0.74 \pm 0.01$

frequency range are also plotted for reference.[44,45,47,48] The QCM-determined moduli correspond to room-temperature measurements conducted between a total frequency range of 5 MHz to 65 MHz for three samples of different film thicknesses. The lower-frequency rheometry data was measured over a frequency range of approximately 10^{-3}–10^{+1} Hz at a range of different temperatures, and then time–temperature shifted to higher frequencies corresponding to a reference temperature of 25 °C. Excellent agreement is obtained between the QCM MHz data and the lower-frequency rheometry data in agreement with time–temperature superposition. Such good agreement between QCM and lower-frequency rheological measurements have also been reported by others.[9,13,49]

3.4 | Continuum physics model applied to rubbery PDMS films

As a second case, we apply our continuum physics model to another rubbery viscoelastic polymer film, polydimethylsiloxane (PDMS), which is also in its glass transition regime at room temperature in the QCM MHz frequency range.[50] The storage and loss moduli are again modeled using Equations (21)–(22), treating the frequency dependence of the shear modulus as linear on a log–log scale. For PDMS, we use the popular Sylgard 184 elastomer kit to make cross-linked PDMS samples (9 to 1 base to cross-linker ratio by mass) with a zero-frequency elastic modulus $E \approx 1.95 \pm 0.19$ MPa.[35,37]

Again to minimize the number of fit parameters in Equations (21)–(22), we use literature data to estimate values for the exponents β' and β'' representing the local slope of $\log(G')$ and $\log(G'')$ versus $\log(f)$ within the QCM frequency range. Unfortunately, even though PDMS is commonly used in various fields such as microfluidics,[51] cell biology,[52,53] soft robotics,[54] and 3D printing,[55] viscoelastic master curves with a wide span of frequencies are scarce. We were able to find DMA data for the same Sylgard 184 PDMS elastomer we use published by Tiwari et al., where they measured the frequency-dependent Young's modulus $E(\omega)$ from −140 °C to 120 °C in 5 °C increments, and then time–temperature shifted the data to create a master curve at a reference temperature of 20 °C.[50] Although this study by Tiwari et al. used slightly different curing conditions and base to cross-linker ratio, our previous literature compilation of Sylgard 184 PDMS Young's modulus values suggests these small differences are not significant, and the Tiwari et al. modulus curve should be a decent representation for our PDMS.[35]

To obtain the storage exponent β' for QCM shear measurements, we converted their Young's modulus $E(\omega)$ data to shear modulus using the simple relation $G'(\omega) = \frac{E(\omega)}{3}$ that assumes Poisson's ratio $\nu = 0.5$. This is a good approximation for rubbery PDMS ($\nu = 0.495$ for Sylgard 184 PDMS[56]), but will cause some discrepancy at higher frequencies when the material is nearly glassy. The MHz frequency range for our PDMS QCM measurements (5–35 MHz) falls within the glass transition regime of PDMS at room temperature. The Tiwari et al. data actually have a gap in this regime because of crystallization issues, thus we have interpolated the $G'(\omega)$ data (see Figure 8) using a simple linear interpolation to connect the rubbery and glassy regimes and estimate a reasonable value for the elastic exponent as $\beta' = 0.32 \pm 0.08$. As loss modulus $G''(\omega)$ data are not available, we performed the Kramers-Kronig transformation on the storage modulus data by Tiwari et al.[50] to obtain $\log G''(f)$ as a function of $\log(f)$ data from which to estimate a β'' value. As outlined in Ref. [57], the Kramers-Kronig transformation for polymer master curves from $G'(f)$ to $G''(f)$ is given by

$$G''(f) = \frac{2f}{\pi} \int_0^\infty \frac{G'(u) - G'(f)}{u^2 - f^2} du, \tag{23}$$

assuming Boltzmann's superposition principle is valid. Even though the Tiwari et al. data already span 30 decades in frequency, we extended the data to infinity assuming a flat glassy and rubbery plateau to account for the limits of integration. The value of β'' determined by fitting the resulting $\log G''$ as a function of $\log f$ curve in the 5–35 MHz frequency range used for QCM measurements of PDMS was $\beta'' = 0.2 \pm 0.1$.

We performed QCM measurements on PDMS films with film thicknesses of 450 nm, 550 nm, and 960 nm. Data on thicker films up to 2 μm were also collected, but lacked clear reliable resonance peaks that could be fit. For the PDMS films, resonance traces over the harmonic range from $n = 1$ to $n = 7$ were collected and fit using Equation (3) to obtain f_n and Γ_n. Figure 7A shows representative resonance traces for a 450 nm thick PDMS film at harmonic numbers $n = 3$, 5, and 7. As expected, we observe that anharmonic side peaks emerge at higher harmonics, which eventually merge with and obscure the main resonance peak. As in the PB case, we have identified resonance traces for PDMS samples where we believe the main resonance peak can still be reliably fit to obtain f_n and Γ_n by limiting the fitting range, like that shown in Figure 7A for $n = 7$. Resonance shifts obtained from such traces have been denoted with open symbols in Figure 7B and 7C, where solid symbols indicate resonance traces with no anharmonic side peaks present. Similar to the PB data, fits of our continuum physics model to the Δf_n and $\Delta\Gamma_n$ resonance shifts using only the data without any

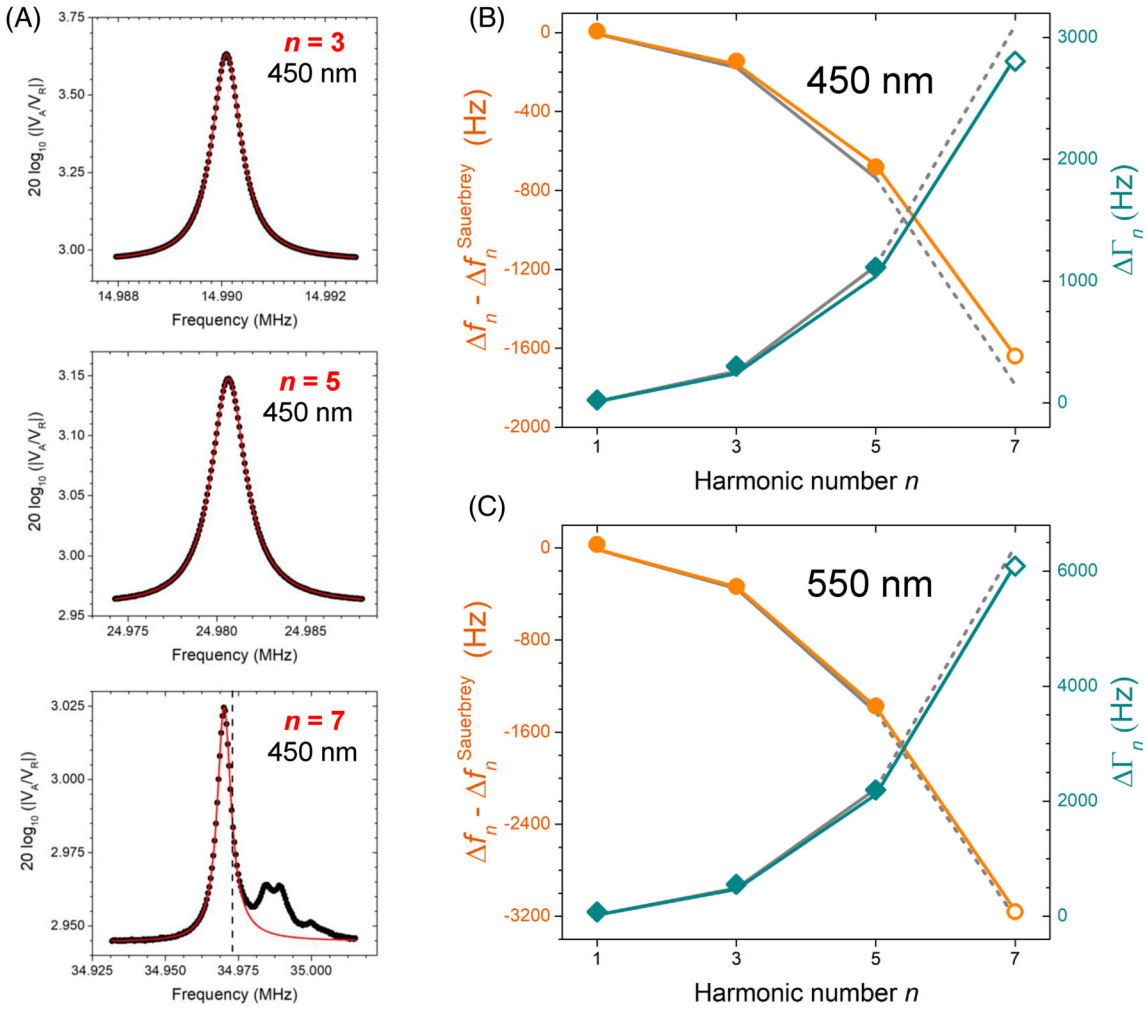

FIGURE 7 (A) QCM resonance traces measured for a 450 nm thick PDMS film at the $n = 3$, 5, and 7 harmonics (symbols), with fits to equation (3) shown as red curves. For the $n = 7$ resonance, data were only fit up to the vertical dashed line. (B) and (C) plot the frequency Δf_n (orange circles, left axis) and dissipation $\Delta\Gamma_n$ (teal diamonds, right axis) shifts for 450 nm and 550 nm thick PDMS films, relative to the expected Sauerbrey mass contribution shift $\Delta f_n^{\text{Sauerbrey}}$. The solid-colored curves are a fit to both the solid and open symbols, while the gray solid and dashed curves are a fit to the solid symbols that are then extrapolated to higher harmonics

anharmonic side peaks (solid symbols) and then extrapolated to higher harmonics, agree well with the open symbols. Thus, we have again chosen to report results that include fits to both the solid and open symbols.

Figure 7B and 7C graph the frequency and dissipation shifts relative to that of the bare quartz, determined as $\Delta f_n = f_n^{\text{film+QCM}} - f_n^{\text{bare QCM}}$ and $\Delta\Gamma_n = \Gamma_n^{\text{film+QCM}} - \Gamma_n^{\text{bare QCM}}$, for 450 nm and 550 nm thick PDMS films. To emphasize the viscoelastic response of these rubbery films, the measured resonance shifts Δf_n and $\Delta\Gamma_n$ for the PDMS films are again plotted relative to the expected shift from only added mass $\Delta f_n^{\text{Sauerbrey}}$ based on the Sauerbrey equation, Equation (1). We fit these data (both solid and open symbols) to our continuum physics model to obtain the storage $G'(n) = G_0' n^{\beta'}$ and loss $G''(n) = G_0'' n^{\beta''}$ moduli, and film thickness h for the PDMS films. In Equations (21)–(22), the exponents were held fixed at $\beta' = 0.32$ and $\beta'' = 0.2$ that we determined from the literature. The density of Sylgard 184 PDMS was taken to be $\rho = 1.1$ g/cm^3.[58] The best fit values from our continuum physics model to all the Δf_n and $\Delta\Gamma_n$ data as a function of harmonic number n are $G_0' = 8.19 \pm 0.81$ MPa, $G_0'' = 12.7 \pm 2.7$ MPa, and $h = 452 \pm 9$ nm for the 450 nm thick PDMS film; $G_0' = 7.99 \pm 0.37$ MPa, $G_0'' = 11.1 \pm 1.7$ MPa, and $h = 548 \pm 12$ nm for the 550 nm thick PDMS film; and $G_0' = 8.29 \pm 0.16$ MPa, $G_0'' = 10.28 \pm 0.89$ MPa, and $h = 960 \pm 10$ nm for the 960 nm thick PDMS film. These film thickness values determined by QCM are in good agreement with the independently measured values by ellipsometry of $h = 468 \pm 3$ nm, $h = 580 \pm 16$ nm, and $h = 972 \pm 4$ nm. As for the PB films, we do not observe any thickness dependence to the moduli values measured by QCM to within experimental error.

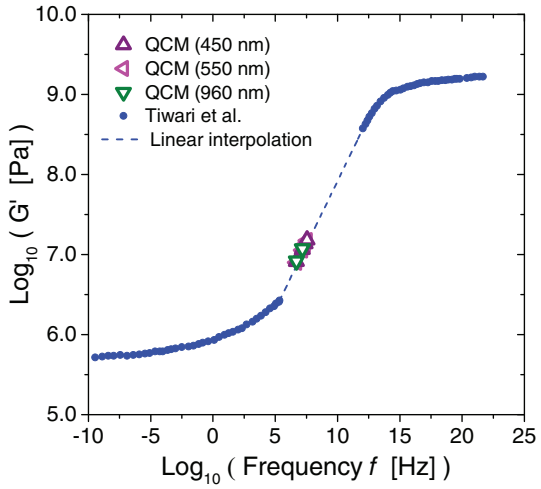

FIGURE 8 Log–log plot of the storage modulus $G'(f)$ for PDMS. Open symbols are the QCM data we measured for Sylgard 184 PDMS films with thicknesses of 450 nm (purple upward-pointing triangles), 550 nm (pink sideward-pointing triangles), and 960 nm (green downward-pointing triangles) in the frequency range of 5 MHz to 35 MHz and at 25 °C. DMA data by Tiwari et al.[50] for Sylgard 184 PDMS, time–temperature shifted to a reference temperature of 20 °C, is also plotted for comparison. The dashed line is a linear interpolation between the rubbery and glassy regimes of the Tiwari et al. data giving a slope of $\beta' = 0.32$

In Figure 8, we graph the best fit values of the storage modulus for the PDMS films measured by QCM by plotting $G'(n) = G'_0 n^{\beta'}$, where the error associated with the fitting and the uncertainty in the exponents β' and β'' are smaller than the symbol size. The DMA data by Tiwari et al.[50] are plotted for comparison. We observe excellent agreement between the storage modulus values measured by QCM for PDMS film thicknesses of 450 nm, 550 nm, and 960 nm in the frequency range of 5 MHz to 35 MHz with the Tiwari et al. DMA data.

4 | CONCLUSIONS

In this study, we have presented a full solution to the shear wave propagation of a MHz QCM acoustic signal through a polymer film subject to the boundary conditions of displacement and stress continuity at the interfaces, retaining the physical intuition of the continuum physics of wave propagation. By leveraging modern computational techniques, we are able to solve the resulting set of three coupled equations without any approximations. Viscoelastic QCM measurements were performed on rubbery polymer films of PB and PDMS near their glass transition regimes, as well as control measurements on glassy PS films. The measured frequency Δf_n and dissipation $\Delta\Gamma_n$ shifts over an extended range of harmonic numbers n were numerically fit to determine the storage $G'(f_n)$ and loss $G''(f_n)$ moduli of the polymer, as well as the film thickness h, from the QCM data. These film thickness values determined from the QCM measurements were found to agree well with values determined by ellipsometry. The frequency dependence of the modulus was treated as linear on a log–log scale over the frequency range of the QCM (5–65 MHz corresponding to n = 1–13) as $\log_{10}G' = \beta' \log_{10} n + \log_{10} G'_0$ and $\log_{10}G'' = \beta'' \log_{10} n + \log_{10} G''_0$. To minimize the number of fitting parameters, the β' and β'' values representing the local slope of the log modulus vs. log frequency data over the QCM frequency range were determined from literature data. The measured storage $G'(f_n)$ and loss $G''(f_n)$ moduli from QCM in the MHz frequency regime for polymer films ranging in thickness from 250 nm to 1.4 μm agreed well with literature rheometry data taken on bulk samples over a frequency range of 10^{-3}–10^{+1} Hz that were time–temperature shifted to higher frequencies. Thus, QCM MHz-frequency viscoelasticity measurements can be used to verify the validity of time–temperature superposition,[1,13] which has been reported to break down at time scales corresponding to MHz frequencies for some polymers.[59]

Taking advantage of the fact that we are numerically solving the resonance frequency Δf_n and dissipation $\Delta\Gamma_n$ shifts exactly, we examine the reliability of data collected at higher harmonics near film resonance. Higher harmonics that approach film resonance are typically avoided because of the belief that the presence of anharmonic side bands make the data unreliable. We test this by comparing the measured Δf_n and $\Delta\Gamma_n$ values at higher harmonics with the expected values based on an extrapolation of the continuum physics model from the data collected at lower harmonics. For QCM resonance traces where we believe the resonance peak can be adequately fit, we find that the measured Δf_n and $\Delta\Gamma_n$ data agree well with the model, even if anharmonic side bands are adjacent to the resonance peak.

ACKNOWLEDGMENTS

Funding from the National Science Foundation polymers program (DMR-1905782) (Connie B. Roth) and Emory University is gratefully acknowledged.

CONFLICT OF INTEREST

The authors have no conflicts of interest to disclose.

ORCID

Yannic J. Gagnon https://orcid.org/0000-0003-0212-3904
Justin C. Burton https://orcid.org/0000-0002-4797-8968
Connie B. Roth https://orcid.org/0000-0002-9543-0614

REFERENCES

[1] K. R. Shull, M. Taghon, Q. Wang, *Biointerphases* **2020**, *15*, 021012.
[2] D. Johannsmann, A. Langhoff, C. Leppin, *Sensors* **2021**, *21*, 3490.
[3] A. D. Easley, T. Ma, C. I. Eneh, J. Yun, R. M. Thakur, J. L. Lutkenhaus, *J. Polym. Sci.* **2021**. https://doi.org/10.1002/pol.20210324
[4] D. Johannsmann, K. Mathauer, G. Wegner, W. Knoll, *Phys. Rev. B* **1992**, *46*, 7808.
[5] A. Domack, O. Prucker, J. Rühe, D. Johannsmann, *Phys. Rev. E* **1997**, *56*, 680.
[6] O. Wolff, D. Johannsmann, *J. Appl. Phys.* **2000**, *87*, 4182.
[7] D. A. Brass, K. R. Shull, *J. Appl. Phys.* **2008**, *103*, 073517.
[8] G. C. DeNolf, L. Haack, J. Holubka, A. Straccia, K. Blohowiak, C. Broadbent, K. R. Shull, *Langmuir* **2011**, *27*, 9873.
[9] G. C. DeNolf, L. F. Sturdy, K. R. Shull, *Langmuir* **2014**, *30*, 9731.
[10] L. Sturdy, F. Casadio, M. Kokkori, K. Muir, K. R. Shull, *Polym. Degrad. Stab.* **2014**, *107*, 348.
[11] L. F. Sturdy, A. Yee, F. Casadio, K. R. Shull, *Polymer* **2016**, *103*, 387.
[12] K. Sadman, C. G. Wiener, R. Weiss, C. C. White, K. R. Shull, B. D. Vogt, *Anal. Chem.* **2018**, *90*, 4079.
[13] D. E. Delgado, L. F. Sturdy, C. W. Burkhart, K. R. Shull, *J. Polym. Sci., Part B: Polym. Phys.* **2019**, *57*, 1246.
[14] D. K. Reid, A. Summers, J. O'Neal, A. V. Kavarthapu, J. L. Lutkenhaus, *Macromolecules* **2016**, *49*, 5921.
[15] H. Furusawa, T. Sekine, T. Ozeki, *Macromolecules* **2016**, *49*, 3463.
[16] X. Tang, J. Fang, X. Du, D.-M. Zhu, *J. Appl. Polym. Sci.* **2017**, *134*, 44532.
[17] H. Tanoue, N. L. Yamada, K. Ito, H. Yokoyama, *Langmuir* **2017**, *33*, 5166.
[18] J. Petri, D. Johannsmann, *Anal. Chem.* **2019**, *91*, 1595.
[19] J. T. O'Neal, E. Y. Dai, Y. Zhang, K. B. Clark, K. G. Wilcox, I. M. George, N. E. Ramasamy, D. Enriquez, P. Batys, M. Sammalkorpi, J. L. Lutkenhaus, *Langmuir* **2018**, *34*, 999.
[20] D. Lin, P. Lopez-Sanchez, N. Selway, M. J. Gidley, *Food Hydrocolloids* **2018**, *79*, 13.
[21] A. D. Monta, F. Razan, J.-B. Le Cam, G. Chagnon, *Sens. Actuators, A* **2018**, *280*, 107.
[22] M. Zhang, C. G. Wiener, P. I. Sepulveda-Medina, J. F. Douglas, B. D. Vogt, *Langmuir* **2019**, *35*, 16612.
[23] L. H. Sperling, *Sound and Vibration Damping with Polymers*, Vol. 424 (Eds: R. D. Corsaro, L. H. Sperling), Washington, DC: ACS Symposium Series, **1990**, p. 5-22, Ch. 1.
[24] V. G. Geethamma, R. Asaletha, N. Kalarikkal, S. Thomas, *Resonance* **2014**, *19*, 821.
[25] V. T. Rathod, *Sensors* **2020**, *20*, 4051.
[26] G. Sauerbrey, *Zeitschrift für Physik* **1959**, *155*, 206.
[27] D. Johannsmann, *The Quartz Crystal Microbalance in Soft Matter Research: Fundamentals and Modeling*, Springer, Switzerland **2015**.
[28] M. V. Voinova, M. Rodahl, M. Jonson, B. Kasemo, *Phys. Scr.* **1999**, *59*, 391.
[29] N. B. Eisele, F. I. Andersson, S. Frey, R. P. Richter, *Biomacromolecules* **2012**, *13*, 2322.
[30] V. E. Granstaff, S. J. Martin, *J. Appl. Phys.* **1994**, *75*, 1319.
[31] D. Johannsmann, *Phys. Chem. Chem. Phys.* **2008**, *10*, 4516.
[32] D. Johannsmann, *Macromol. Chem. Phys.* **1999**, *200*, 501.
[33] E. J. Martin, M. T. Mathew, K. R. Shull, *Langmuir* **2015**, *31*, 4008.
[34] C. Lu, O. Lewis, *J. Appl. Phys.* **1972**, *43*, 4385.
[35] Y. J. Gagnon, C. B. Roth, *ACS Macro Lett.* **2020**, *9*, 1625.
[36] C. M. Stafford, B. D. Vogt, C. Harrison, D. Julthongpiput, R. Huang, *Macromolecules* **2006**, *39*, 5095.
[37] E. A. Wilder, S. Guo, S. Lin-Gibson, M. J. Fasolka, C. M. Stafford, *Macromolecules* **2006**, *39*, 4138.
[38] X. Huang, C. B. Roth, *J. Chem. Phys.* **2016**, *144*, 234903.
[39] B. Lautrup, *Physics of Continuous Matter*, 2nd ed., CRC Press, Boca Raton, FL **2011**.
[40] J. Brandrup, E. H. Immergut, E. A. Grulke, A. Abe, D. H. Bloch Eds., *Polymer Handbook*, 4th ed., Wiley, New York **1999**.
[41] P. H. Mott, J. R. Dorgan, C. M. Roland, *J. Sound Vib.* **2008**, *312*, 572.
[42] B. Hartmann, in *Acoustic Properties* (Ed: J. E. Mark), AIP Press, New York **1996**, p. 677.
[43] B. Hartmann, J. Jarzynski, *J. Acoust. Soc. Am.* **1974**, *56*, 1469.
[44] R. H. Colby, L. J. Fetters, W. W. Graessley, *Macromolecules* **1987**, *20*, 2226.
[45] L. I. Palade, V. Verney, P. Attané, *Macromolecules* **1995**, *28*, 7051.
[46] S. J. Park, P. S. Desai, X. Chen, R. G. Larson, *Macromolecules* **2015**, *48*, 4122.
[47] S. Wang, S.-Q. Wang, A. Halasa, W.-L. Hsu, *Macromolecules* **2003**, *36*, 5355.
[48] C.-Y. Liu, R. Keunings, C. Bailly, *Macromolecules* **2007**, *40*, 2946.
[49] L. Szántó, R. Vogt, J. Meier, D. Auhl, E. Van Ruymbeke, C. Friedrich, *J. Rheol.* **2017**, *61*, 1023.
[50] A. Tiwari, L. Dorogin, A. I. Bennett, K. D. Schulze, W. G. Sawyer, M. Tahir, G. Heinrich, B. N. J. Persson, *Soft Matter* **2017**, *13*, 3602.
[51] J. M. K. Ng, I. Gitlin, A. D. Stroock, G. M. Whitesides, *Electrophoresis* **2002**, *23*, 3461.
[52] J. N. Lee, X. Jiang, D. Ryan, G. M. Whitesides, *Langmuir* **2004**, *20*, 11684.
[53] M. Murrell, R. Kamm, P. Matsudaira, *Biophys. J.* **2011**, *101*, 297.
[54] G. M. Whitesides, *Angewandte Chem. Int. Ed.* **2018**, *57*, 4258.
[55] J. Herzberger, J. M. Sirrine, C. B. Williams, T. E. Long, *Prog. Polym. Sci.* **2019**, *97*, 101144.
[56] A. Müller, M. C. Wapler, U. Wallrabe, *Soft Matter* **2019**, *15*, 779.
[57] H. C. Booij, G. P. J. M. Thoone, *Rheol. Acta* **1982**, *21*, 15.
[58] L. L. Stevens, E. B. Orler, D. M. Dattelbaum, M. Ahart, R. J. Hemley, *J. Chem. Phys.* **2007**, *127*, 104906.
[59] Y. Ding, A. P. Sokolov, *Macromolecules* **2006**, *39*, 3322.

SUPPORTING INFORMATION

Additional supporting information may be found in the online version of the article at the publisher's website.

How to cite this article: Y. J. Gagnon, J. C. Burton, C. B. Roth, *J. Polym. Sci.* **2022**, *60*(2), 244. https://doi.org/10.1002/pol.20210763